Karlsruhe Institute of Technology

école normale supérieure paris–saclay

Analysis and optimization of ray-based 3D Ultrasound Tomography

Workshop ARPE

Pierre-Antoine Comby | September 17, 2020

INSTITUT FOR DATA PROCESSING AND ELECTRONICS

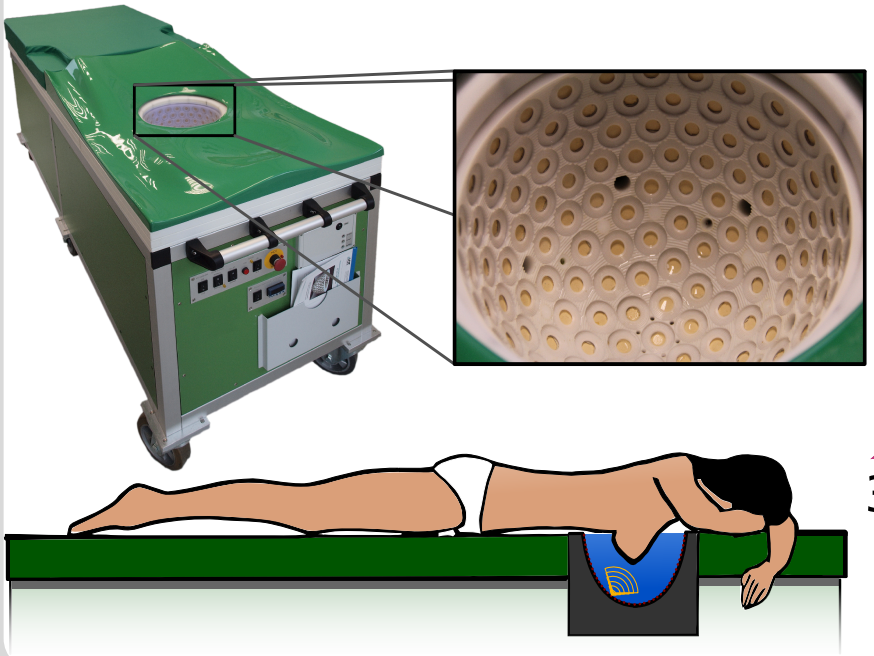

USCT

3D Ultrasound Computer Tomography

USCT Project

Groundwork

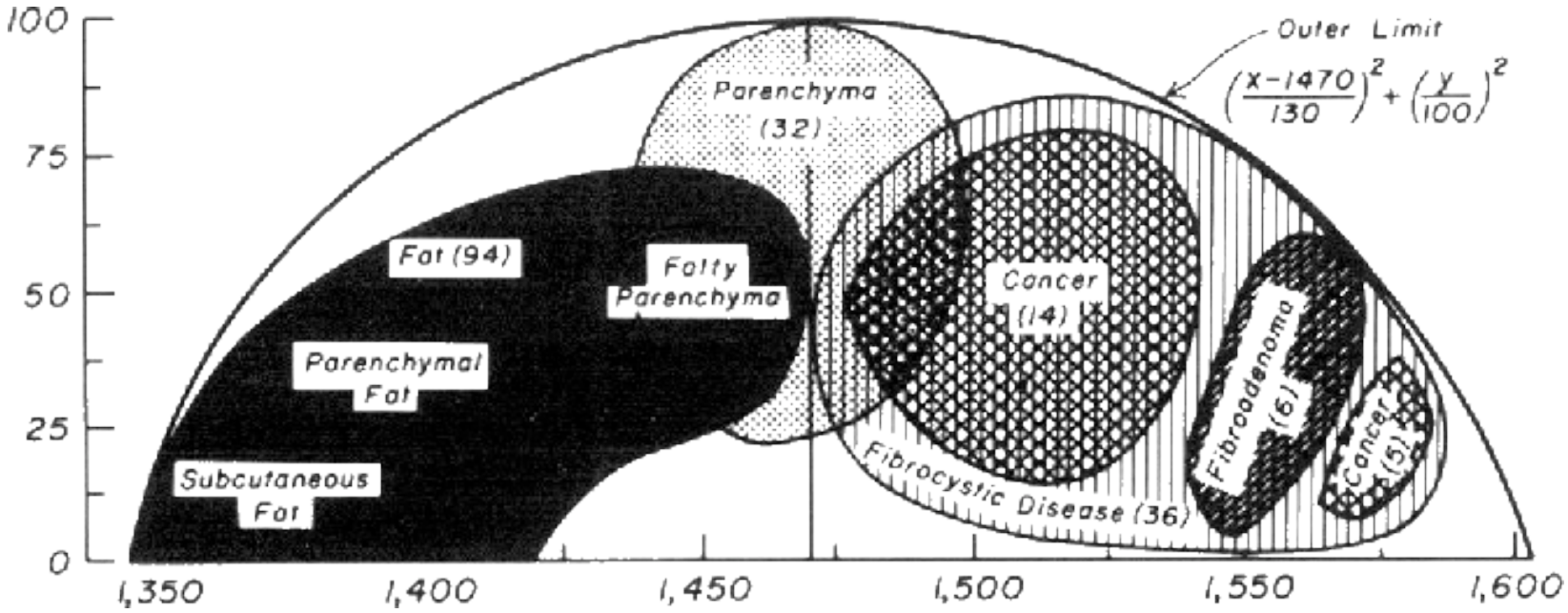

Figure 1: Acoustic characteristic of breast tissues: Attenuation/Velocity

Ultrasonic Computed Tomography

USCT Project

Groundwork

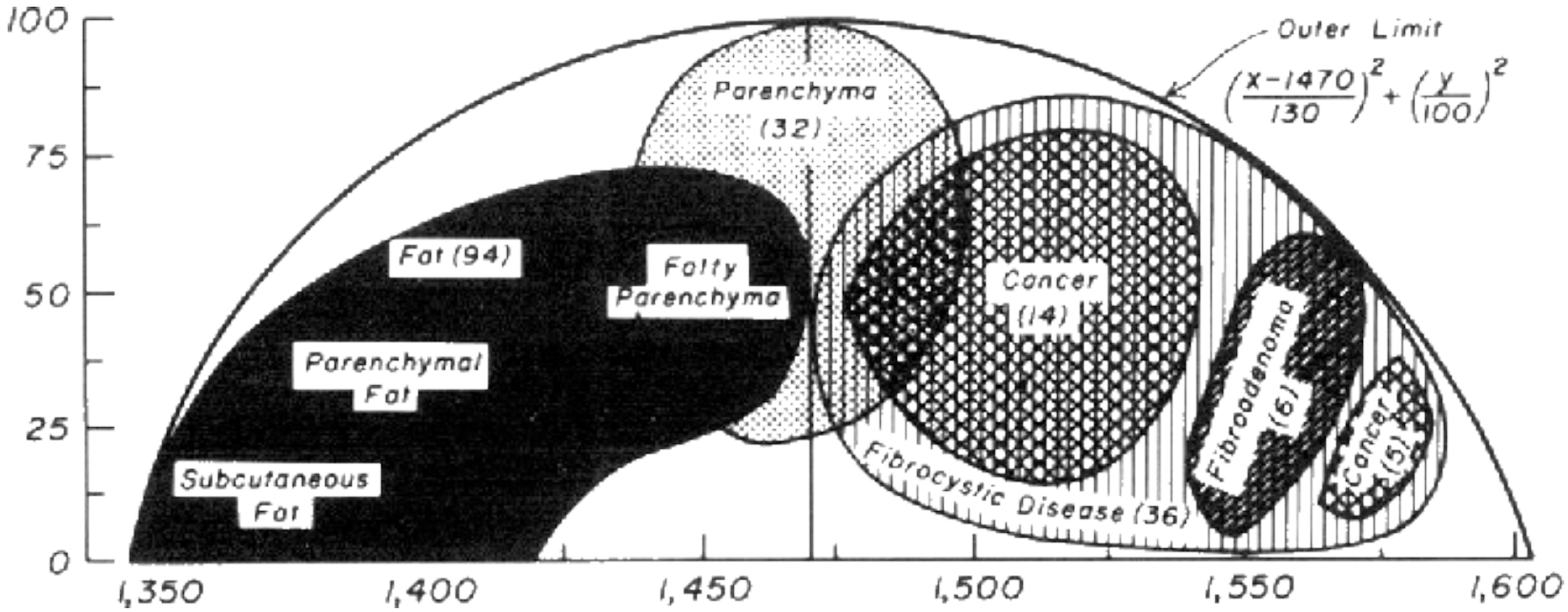

Figure 1: Acoustic characteristic of breast tissues: Attenuation/Velocity

Ultrasonic Computed Tomography

- 3D (world premiere)
- High resolution (tumour $<$5mm)
- Multi-modal imaging

USCT Project

Groundwork

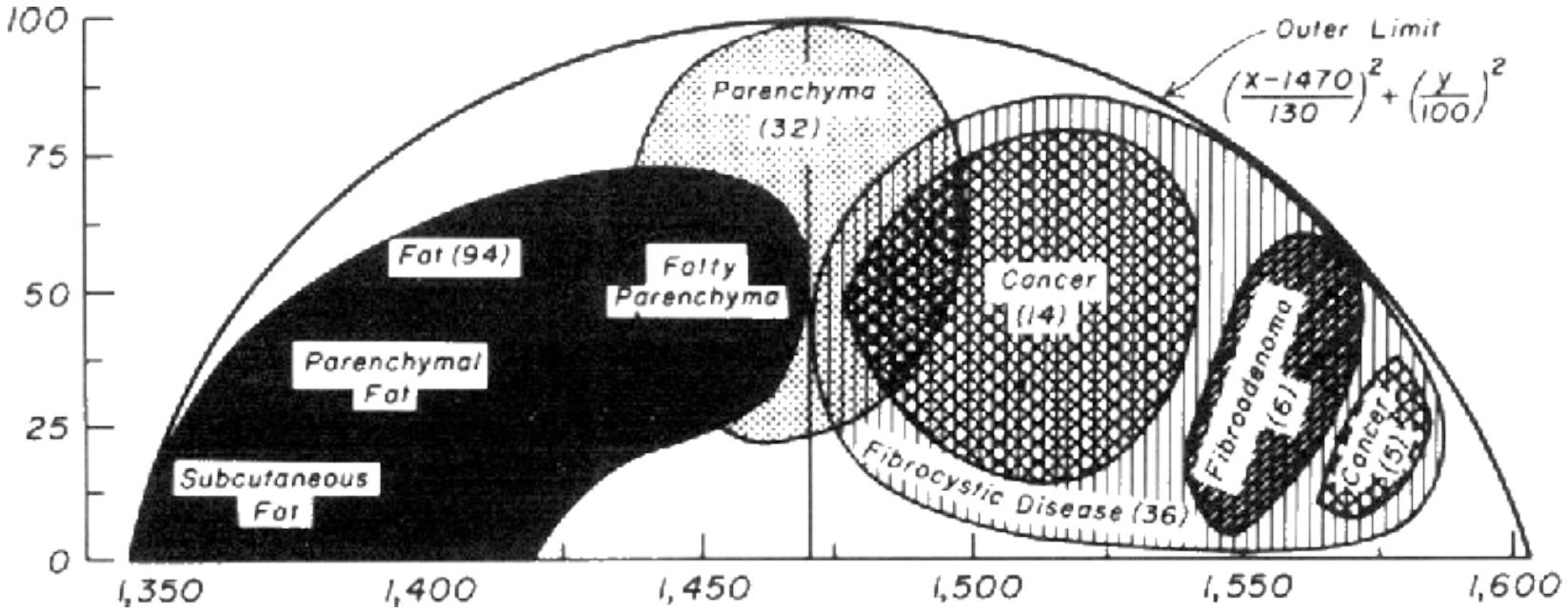

Figure 1: Acoustic characteristic of breast tissues: Attenuation/Velocity

Ultrasonic Computed Tomography

- 3D (world premiere)
- High resolution (tumour $<$5mm)
- Multi-modal imaging
- no uses of X-rays
- Cost effective

USCT Project

Device Principle

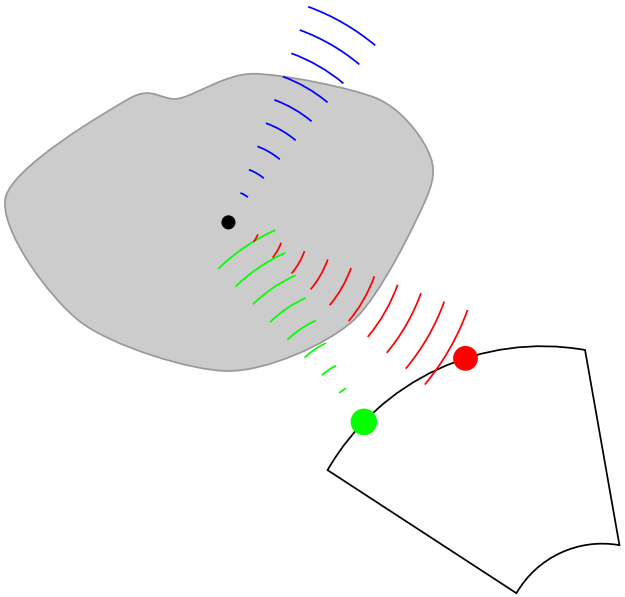

(a) 2D

USCT Project

Device Principle

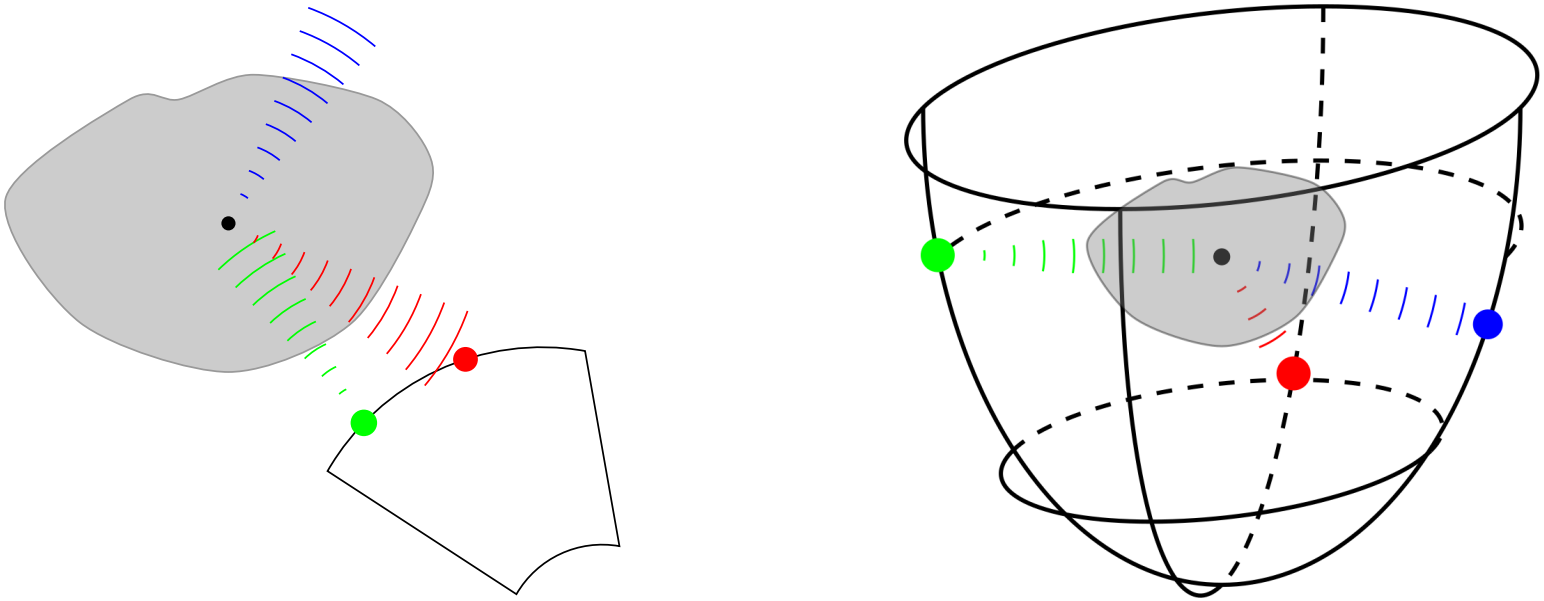

(a) 2D

(b) 3D

Figure 2: 2D vs 3D Tomography

USCT Project

Device Principle

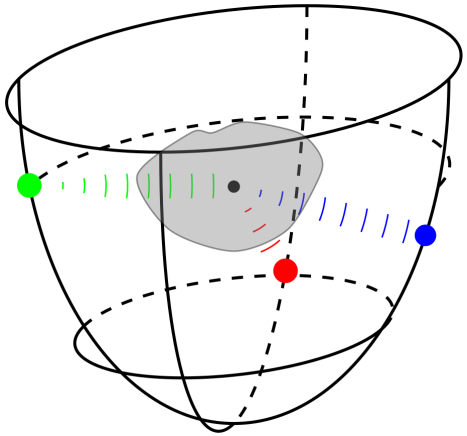

Figure 3: 3D Tomography

- Acoustics measurements
  - **Speed of sound**
  - Attenuation
  - Reflectivity

USCT Project

Device Principle

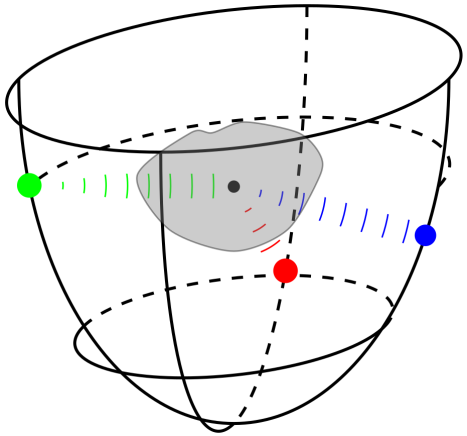

Figure 3: 3D Tomography

- Acoustics measurements
  - **Speed of sound**
  - Attenuation
  - Reflectivity

Simulation Framework

- 2D High Res. acquisition simulation
  - Groundtruth: 1px = 0.1 mm

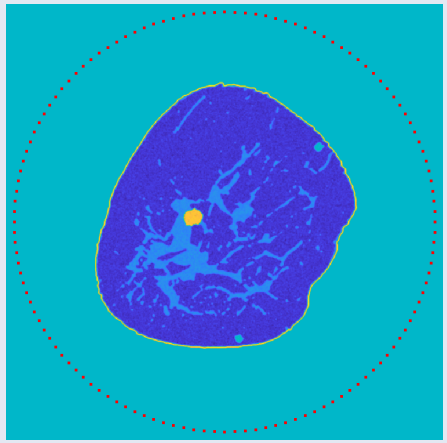

USCT Project

Device Principle

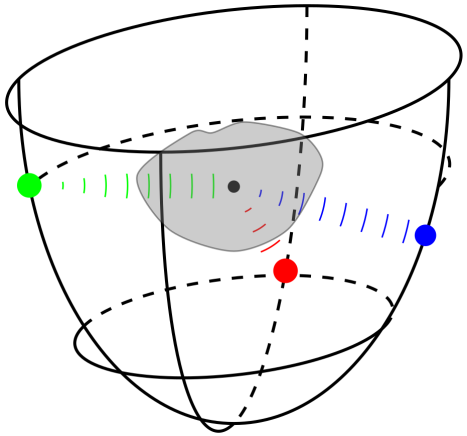

Figure 3: 3D Tomography

- Acoustics measurements
  - **Speed of sound**
  - Attenuation
  - Reflectivity

Simulation Framework

- 2D High Res. acquisition simulation
  - Groundtruth: 1px = 0.1 mm
  - Based on segmented coronal MRI image

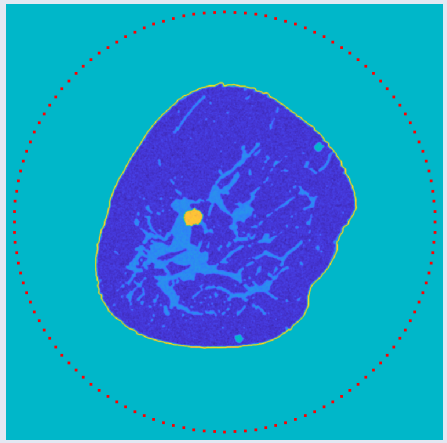

USCT Project

Device Principle

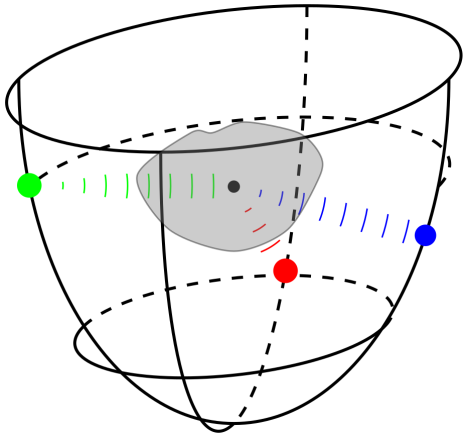

Figure 3: 3D Tomography

- Acoustics measurements
  - **Speed of sound**
  - Attenuation
  - Reflectivity

Simulation Framework

- 2D High Res. acquisition simulation
  - Groundtruth: 1px = 0.1 mm
  - Based on segmented coronal MRI image
- Compress Pulse f=2.5MHz

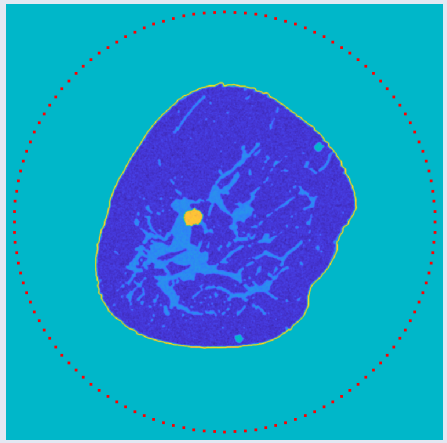

USCT Project

Device Principle

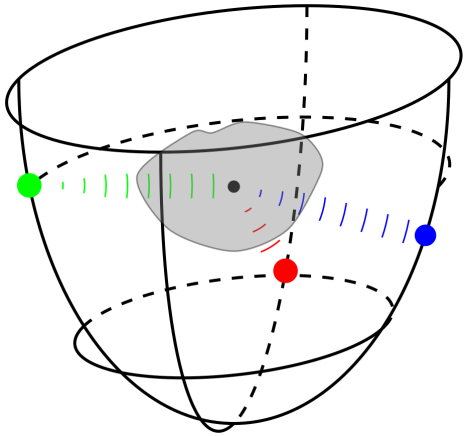

Figure 3: 3D Tomography

- Acoustics measurements
  - **Speed of sound**
  - Attenuation
  - Reflectivity

Simulation Framework

- 2D High Res. acquisition simulation
  - Groundtruth: 1px = 0.1 mm
  - Based on segmented coronal MRI image
- Compress Pulse f=2.5MHz
  - $\nearrow f \implies \searrow$ px size

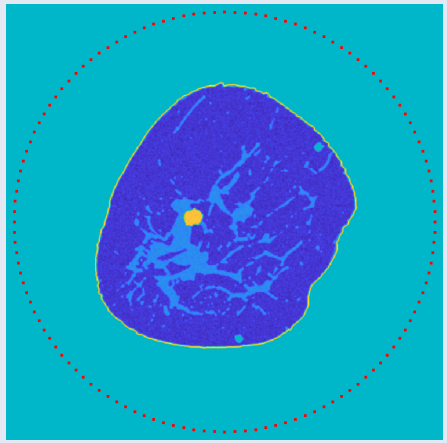

USCT Project

Device Principle

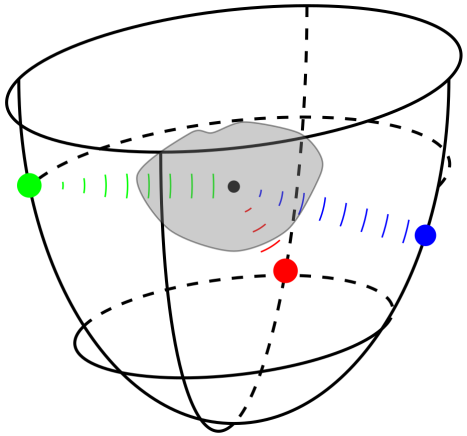

Figure 3: 3D Tomography

- Acoustics measurements
  - **Speed of sound**
  - Attenuation
  - Reflectivity

Simulation Framework

- 2D High Res. acquisition simulation
  - Groundtruth: 1px = 0.1 mm
  - Based on segmented coronal MRI image
- Compress Pulse f=2.5MHz
  - $\nearrow f \implies \searrow$ px size
  - $\searrow f \implies \nearrow$ SNR and depth of field

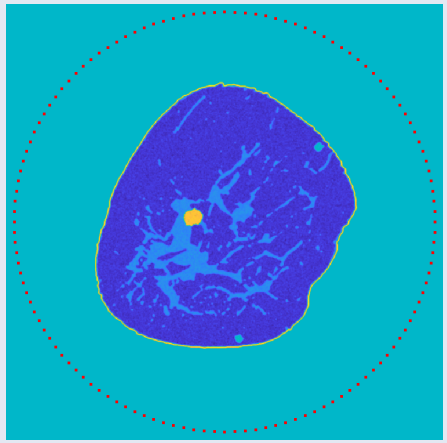

Physics and Modelling

Transmission and Reflection Tomography

Speed of sound tomography

$$c = \frac{\Delta L}{\Delta t} \longrightarrow t = \int \frac{1}{c} \mathrm{d}l$$

- Transmission tomography
- *a priori* for Reflexion tomography

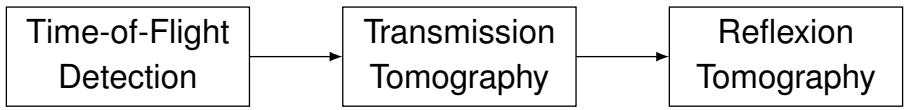

Figure 4: Reconstruction steps for USCT

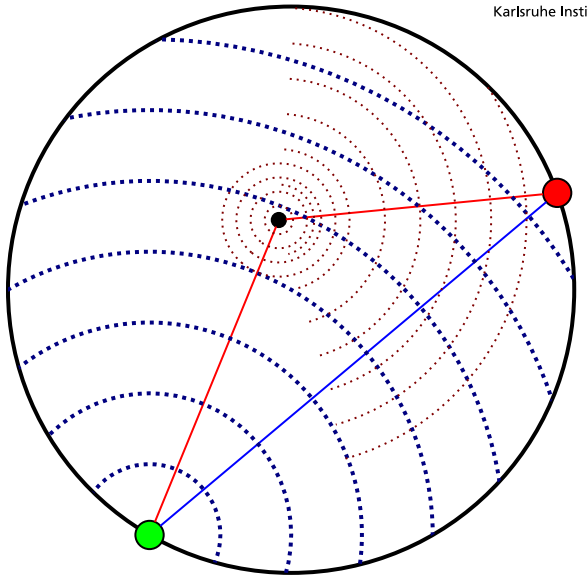

(a) Wave propagation in USCT.

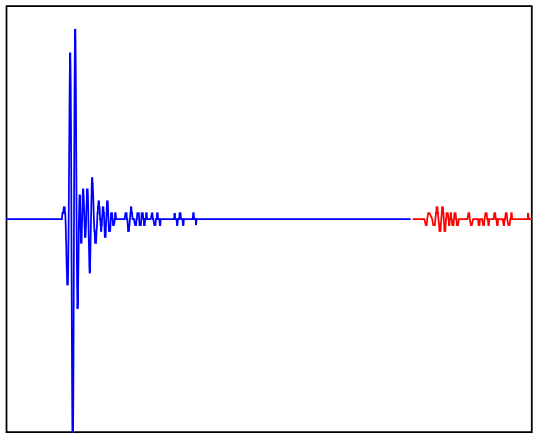

(b) A-Scan acquisition at Receiver.

Figure 5: Data acquisition in 2D

Physics and Modelling

Karlsruhe Institute of Technology

Base equations

- Wave Equation (Fourier Space, $k = \omega / c(\boldsymbol{x})$)

$$\nabla^2 P(\boldsymbol{x}, \omega) + k^2 P(\boldsymbol{x}, \omega) = 0$$

Physics and Modelling

Base equations

- Wave Equation (Fourier Space, $k = \omega / c(\boldsymbol{x})$)

$$\nabla^2 P(\boldsymbol{x}, \omega) + k^2 P(\boldsymbol{x}, \omega) = 0$$

- Assuming an infinite frequency: A *ray* between an emitter and a receiver verifies the *Eikonal Equation*

$$\frac{\mathrm{d}}{\mathrm{d}l} = \left(\frac{1}{c} \frac{\mathrm{d}\boldsymbol{x}}{\mathrm{d}l} \right) = \nabla \left(\frac{1}{c} \right)$$

$$t = \int_{\mathcal{R}} \frac{1}{c} \mathrm{d}l$$

Physics and Modelling

Base equations

- Wave Equation (Fourier Space, $k = \omega / c(\boldsymbol{x})$)

$$\nabla^2 P(\boldsymbol{x}, \omega) + k^2 P(\boldsymbol{x}, \omega) = 0$$

- Assuming an infinite frequency: A *ray* between an emitter and a receiver verifies the *Eikonal Equation*

$$\frac{\mathrm{d}}{\mathrm{d}l} = \left(\frac{1}{c} \frac{\mathrm{d}\boldsymbol{x}}{\mathrm{d}l} \right) = \nabla \left(\frac{1}{c} \right)$$

$$t = \int_{\mathcal{R}} \frac{1}{c} \mathrm{d}l$$

Physics and Modelling

Base equations

- Wave Equation (Fourier Space, $k = \omega / c(\boldsymbol{x})$)

$$\nabla^2 P(\boldsymbol{x}, \omega) + k^2 P(\boldsymbol{x}, \omega) = 0$$

- Assuming an infinite frequency: A *ray* between an emitter and a receiver verifies the *Eikonal Equation*

$$\frac{\mathrm{d}}{\mathrm{d}l} = \left(\frac{1}{c} \frac{\mathrm{d}\boldsymbol{x}}{\mathrm{d}l} \right) = \nabla \left(\frac{1}{c} \right)$$

$$t = \int_{\mathcal{R}} \frac{1}{c} \mathrm{d}l$$

- A ray is the fastest path between an Emitter and a Receiver.

Physics and Modelling

Base equations

- Wave Equation (Fourier Space, $k = \omega / c(\boldsymbol{x})$)

$$\nabla^2 P(\boldsymbol{x}, \omega) + k^2 P(\boldsymbol{x}, \omega) = 0$$

- Assuming an infinite frequency: A *ray* between an emitter and a receiver verifies the *Eikonal Equation*

$$\frac{\mathrm{d}}{\mathrm{d}l} = \left(\frac{1}{c} \frac{\mathrm{d}\boldsymbol{x}}{\mathrm{d}l} \right) = \nabla \left(\frac{1}{c} \right)$$

$$t = \int_{\mathcal{R}} \frac{1}{c} \mathrm{d}l$$

- A ray is the fastest path between an Emitter and a Receiver.
- ray path $\mathcal{R}$ *and* speed of sound unknown.

Physics and Modelling

Infinite frequency rays

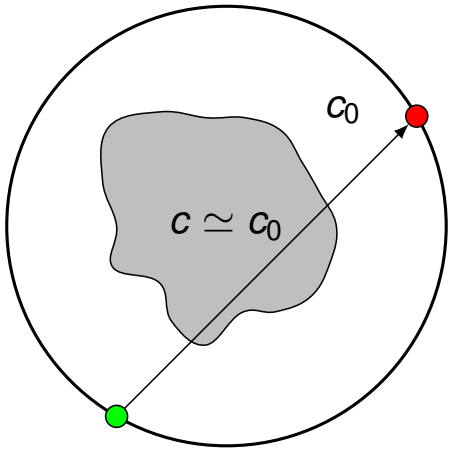

(a) Straight rays

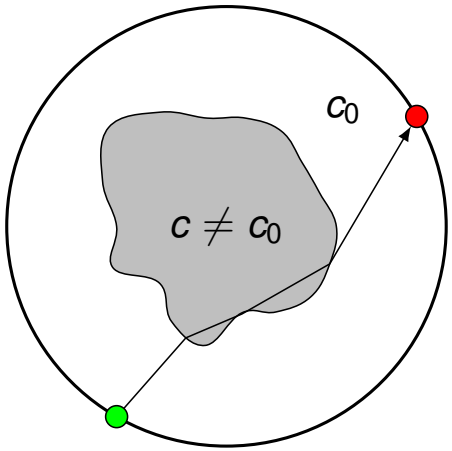

(b) Bent rays

Figure 6: Simples rays approximations

Straight Rays

- Homogeneous medium
- shortest path = fastest path
- Bresenham Line's Algorithm

Bent Rays

- Heterogeneous medium
- shortest path $\neq$ fastest path
- Use Fast Marching Map (FMM) to compute the path

Numerical approximations

- Differential Approach

$$\delta t = \int_{\mathcal{R}} (s(\boldsymbol{x}) - s_0)\,\mathrm{d}l = \int_{\mathcal{R}} \frac{1}{c(\boldsymbol{x})} - \frac{1}{c_0}\mathrm{d}l$$

- Discrete space, for the k-th ray:

$$\delta t_k = \sum_{i=1}^{n_k} l_{ki}\delta s_i$$

- matrix formalism:

$$\underbrace{\begin{bmatrix}\delta t_1\\ \delta t_2\\ \vdots\\ \delta t_m\end{bmatrix}}_{\boldsymbol{y}} = \underbrace{\begin{bmatrix} l_{11} & l_{12} & \cdots & l_{1n}\\ l_{21} & l_{22} & \cdots & l_{2n}\\ \vdots & \vdots & \ddots & \vdots\\ l_{m1} & l_{m2} & \cdots & l_{mn}\end{bmatrix}}_{\boldsymbol{M}} \cdot \underbrace{\begin{bmatrix}\delta s_1\\ \delta s_2\\ \vdots\\ \delta s_n\end{bmatrix}}_{\boldsymbol{\delta s}} \longrightarrow \delta \boldsymbol{y} = \underbrace{\boldsymbol{M}\,\mathcal{I}(\boldsymbol{c})}_{\mathcal{M}}$$

Matrix construction

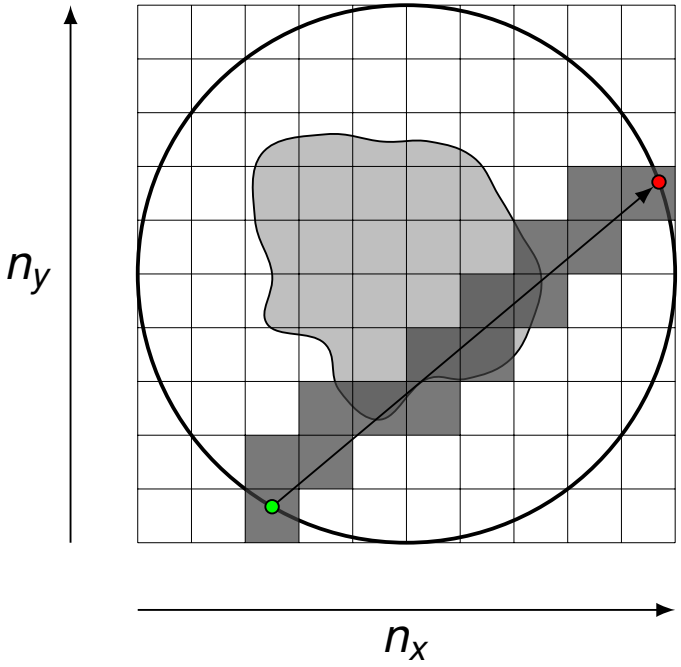

by construction, ***M*** is sparse.
(99% of coefficient are zeros in 2D)

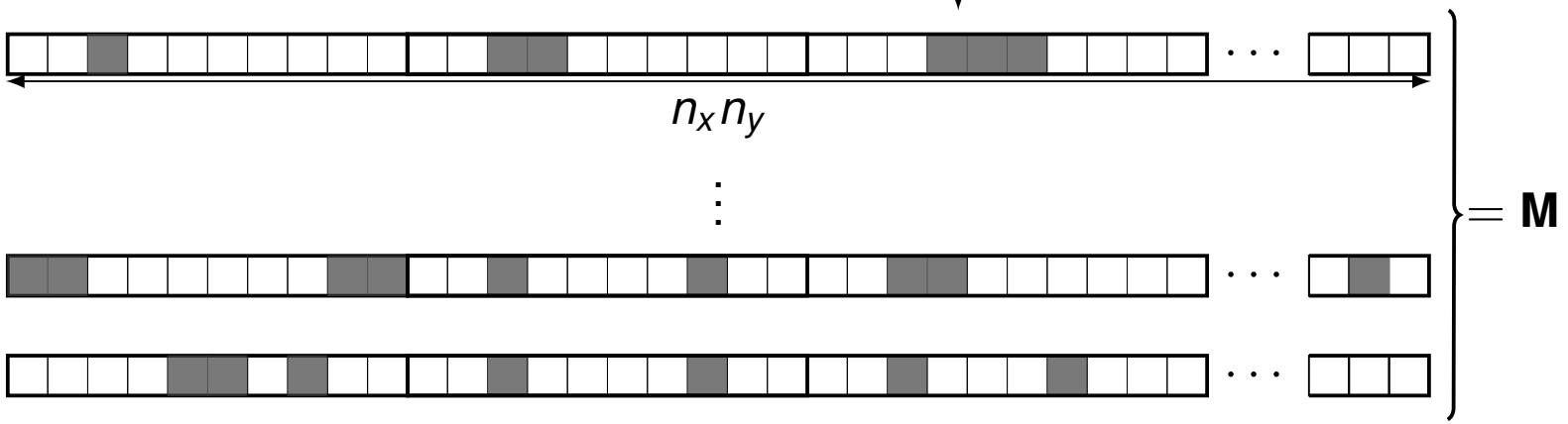

Finite frequency tomography

Introduction

Drawbacks of infinite frequency tomography

- Important sparsity
- High sensibility to noise
- Mathematical conception, no physical origins

Finite frequency tomography

Introduction

Drawbacks of infinite frequency tomography

- Important sparsity
- High sensibility to noise
- Mathematical conception, no physical origins

To solve these problems, Introducing the:

Finite Frequency Tomography

- Theory stolen to geophysics and petrol prospectors
- A step towards *full-wave* approach
- Consider the complete Fresnel Zone for information

Finite frequency tomography

Defining the Fresnel zone

Fresnel Zone

The Fresnel is the region of space who interact constructively on the received wave

$$\delta\tau(F) = \tau(EF) + \tau(FR) - \tau(ER) \leq \frac{1}{2f}$$

Where $\tau(EF), \tau(FR), \tau(ER)$, are the time of flight on the according paths.

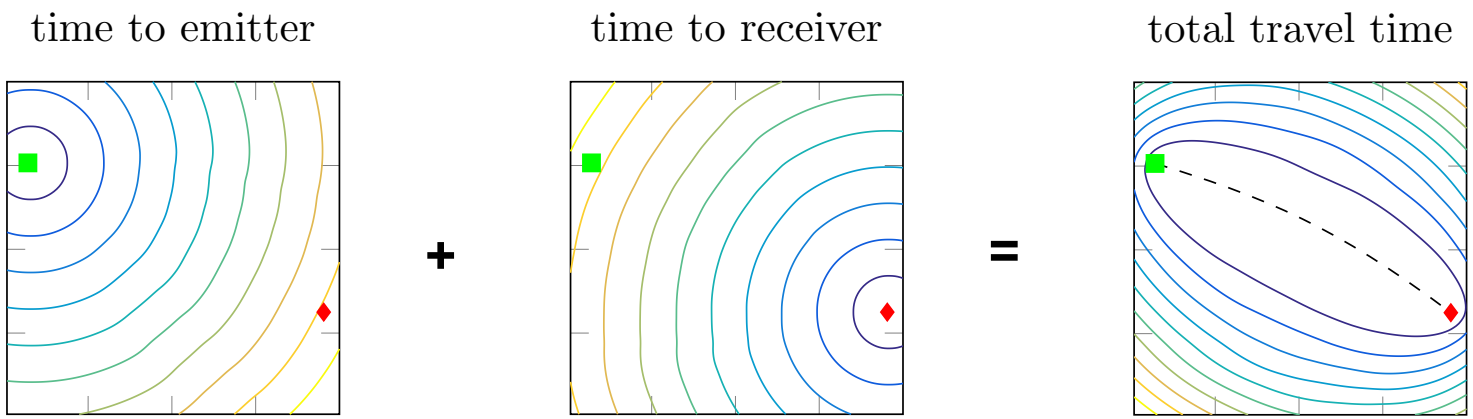

Finite frequency tomography

Fat ray Kernel

In the Fresnel Zone we defines a *sensibility Kernel*

$$\delta t_k = \int_V \delta K_{t_k}(\boldsymbol{x}) \delta s(\boldsymbol{x}) \mathrm{d}x$$

Finite frequency tomography

Fat ray Kernel

In the Fresnel Zone we defines a *sensibility Kernel*

$$\delta t_k = \int_V \delta K_{t_k}(\boldsymbol{x}) \delta s(\boldsymbol{x}) \mathrm{d}x$$

- $K_{t_k,i} \simeq \frac{\partial t_k}{\partial c_i}$ sensitivity
- Different weights methods for fat Ray

Finite frequency tomography

Fat ray Kernel

In the Fresnel Zone we defines a *sensibility Kernel*

$$\delta t_k = \int_V \delta K_{t_k}(\boldsymbol{x}) \delta s(\boldsymbol{x}) \mathrm{d}x$$

- $K_{t_k,i} \simeq \frac{\partial t_k}{\partial c_i}$ sensitivity
- Different weights methods for fat Ray

Naive approach: Spread value of bent ray /straight ray

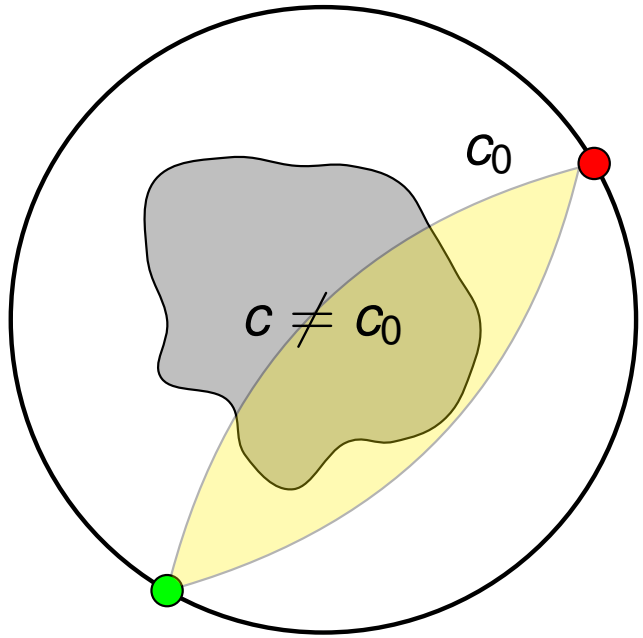

Figure 7: Fresnel Zone for Fat Ray

Finite frequency tomography

Fat ray Kernel

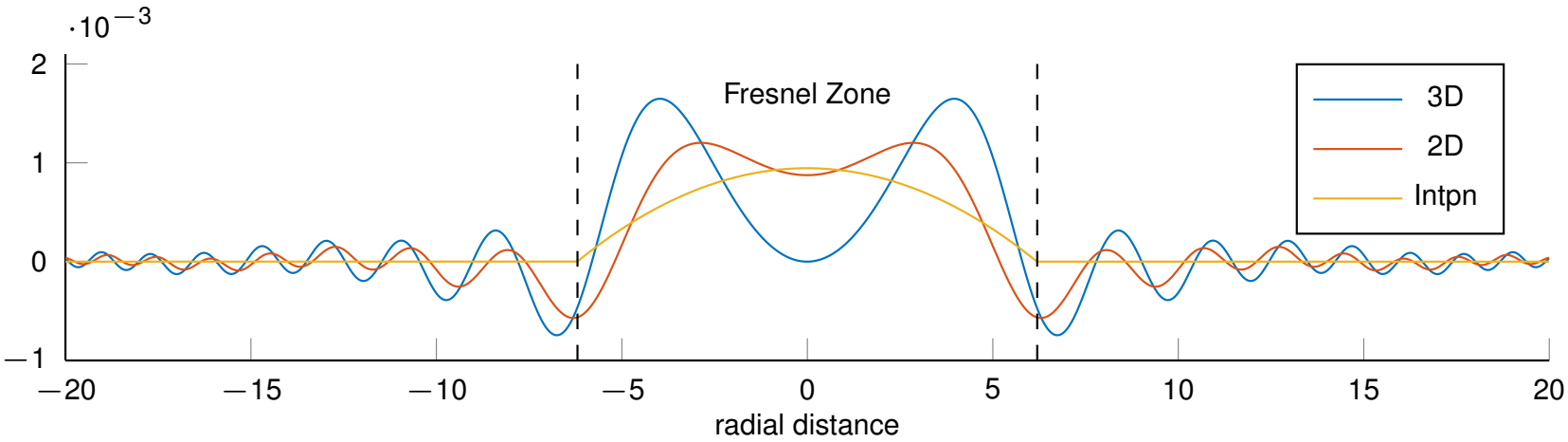

Figure 8: Comparison of Fat ray kernels

- Linear Interpolated Kernel very naive
- Fréchet Kernel (Born/Rytov Approximation)

Problem parameters

Matrix Analysis

Transducer limitations

- Opening angle (real $\simeq 30^o$)
- Number of ray = (Number of Transducer)^2
- Geometrical Artifacts

Problem parameters

Matrix Analysis

Transducer limitations

- Opening angle (real $\simeq 30^o$)
- Number of ray = (Number of Transducer)^2
- Geometrical Artifacts

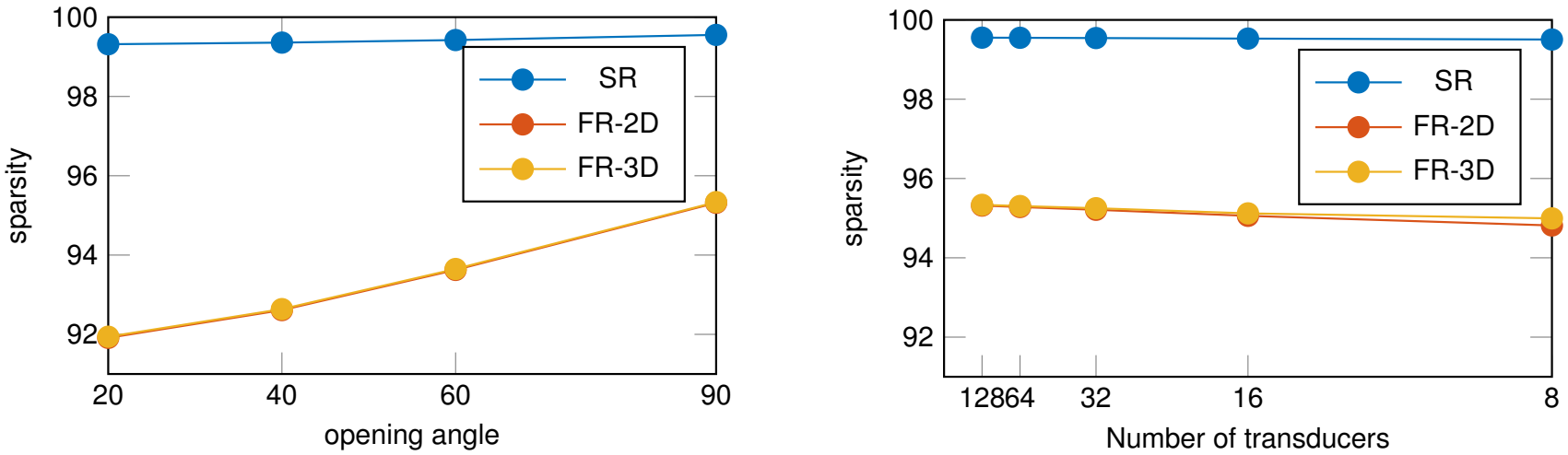

Figure 9: Sparsity of Matrix for different ray methods

Solver design

Inverse Problem

- ill-posed problem $M \neq N$
- ill conditioned $\xi(\boldsymbol{M}) > 10^{10}$ (good value < 10)

Solver design

Inverse Problem

- ill-posed problem $M \neq N$
- ill conditioned $\xi(\boldsymbol{M}) > 10^{10}$ (good value < 10)
- M is sparse
- M is big (memory problems)

Solver design

Inverse Problem

- ill-posed problem $M \neq N$
- ill conditioned $\xi(\boldsymbol{M}) > 10^{10}$ (good value < 10)
- M is sparse
- M is big (memory problems)

$$\boldsymbol{y} = \boldsymbol{M}\boldsymbol{x}$$

Solver design

Inverse Problem

- ill-posed problem $M \neq N$
- ill conditioned $\xi(\boldsymbol{M}) > 10^{10}$ (good value < 10)
- M is sparse
- M is big (memory problems)

$$\boldsymbol{y} = \boldsymbol{M}\boldsymbol{x} \longrightarrow \arg\min_{\boldsymbol{x}} \{f(\boldsymbol{x}, \boldsymbol{y}) + g(\boldsymbol{x})\}$$

Solver design

Inverse Problem

- ill-posed problem $M \neq N$
- ill conditioned $\xi(\boldsymbol{M}) > 10^{10}$ (good value < 10)
- M is sparse
- M is big (memory problems)

$$\boldsymbol{y} = \boldsymbol{M}\boldsymbol{x} \longrightarrow \arg\min_{\boldsymbol{x}} \{f(\boldsymbol{x}, \boldsymbol{y}) + g(\boldsymbol{x})\}$$

Solvers:

- SART (well known)
- TVAL3 (complex to tune)

Region of Interest

Our interest

- Focus computation on the center of the aperture
- Faster
- Less background noise
- Memory efficient

Figure 10: Binary segmentation for ROI detection

Reconstruction Procedure

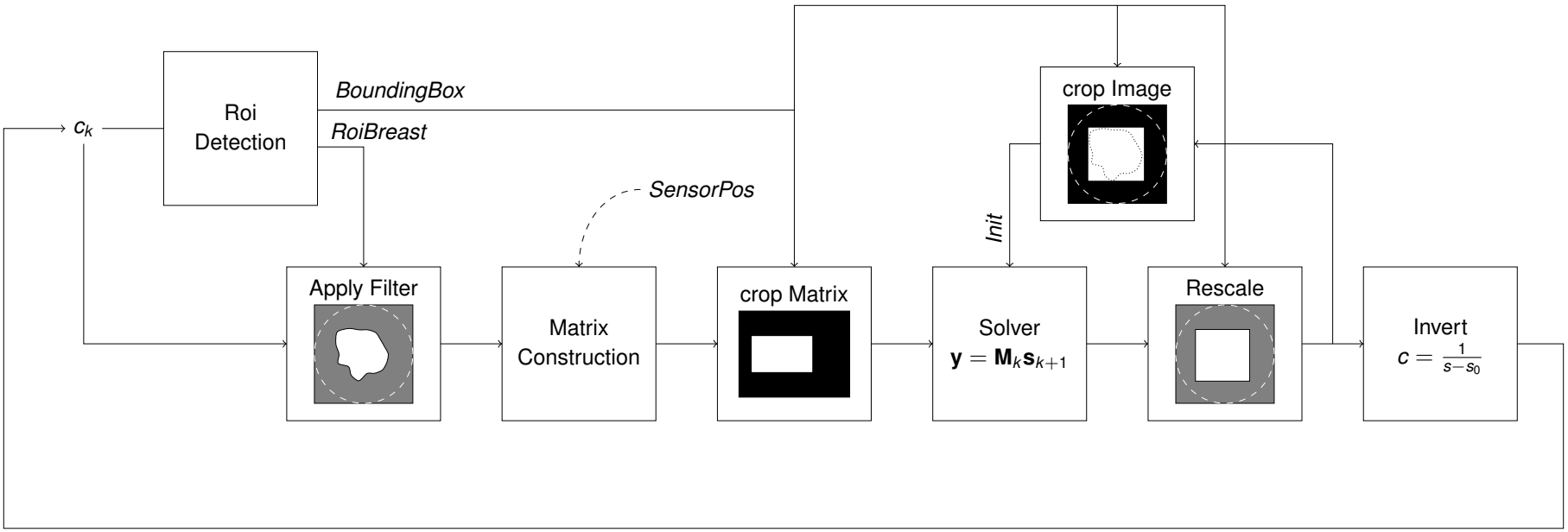

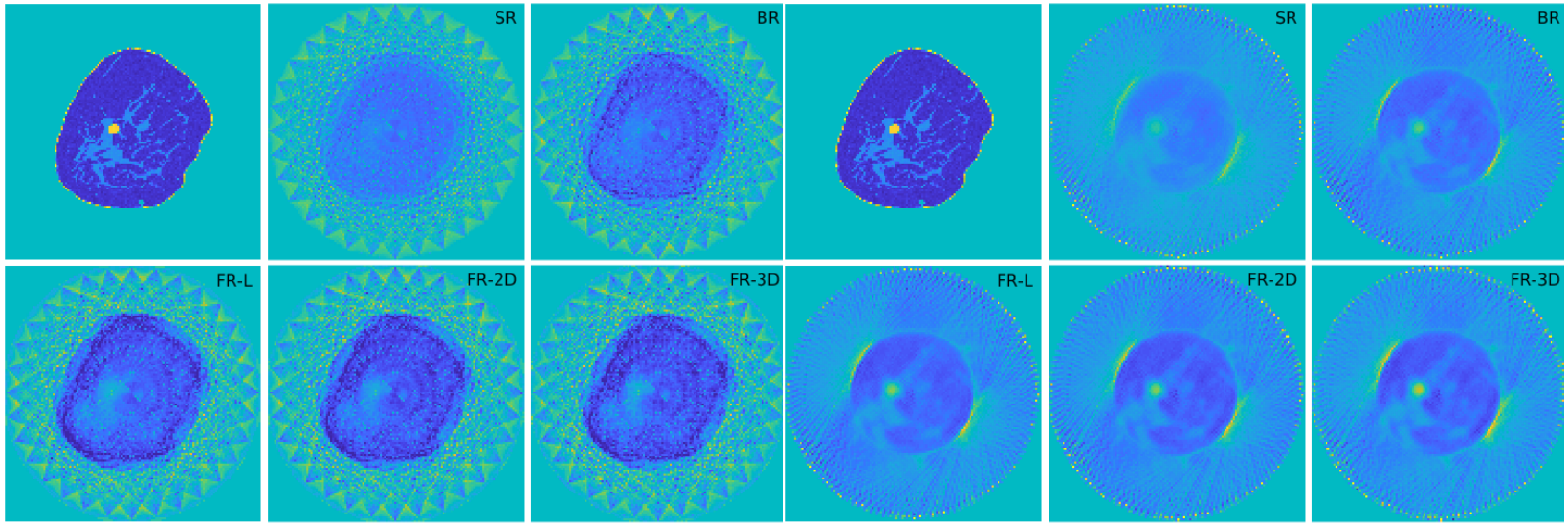

(a) 32 transducers, 90° opening.

(b) 128 transducers, 30° opening.

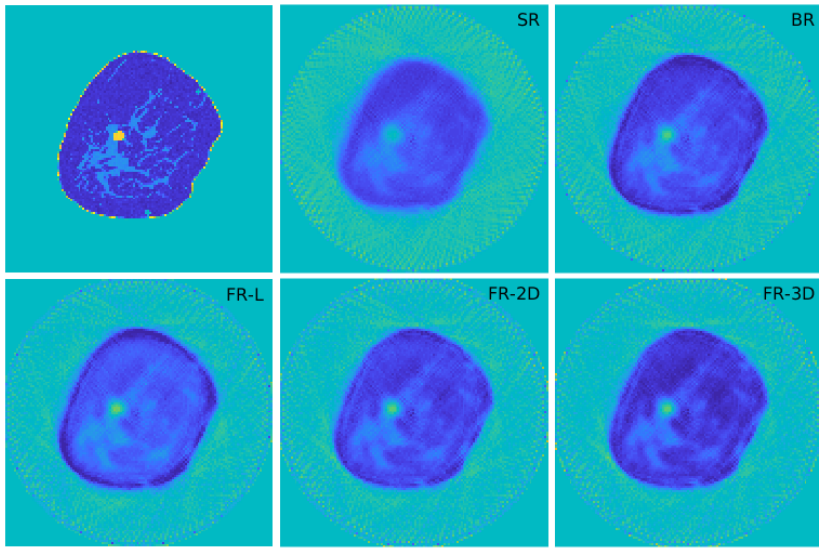

(c) 128 transducers, 90° opening.

Figure 11: Opening and Number of Rays Influence

Results

SART

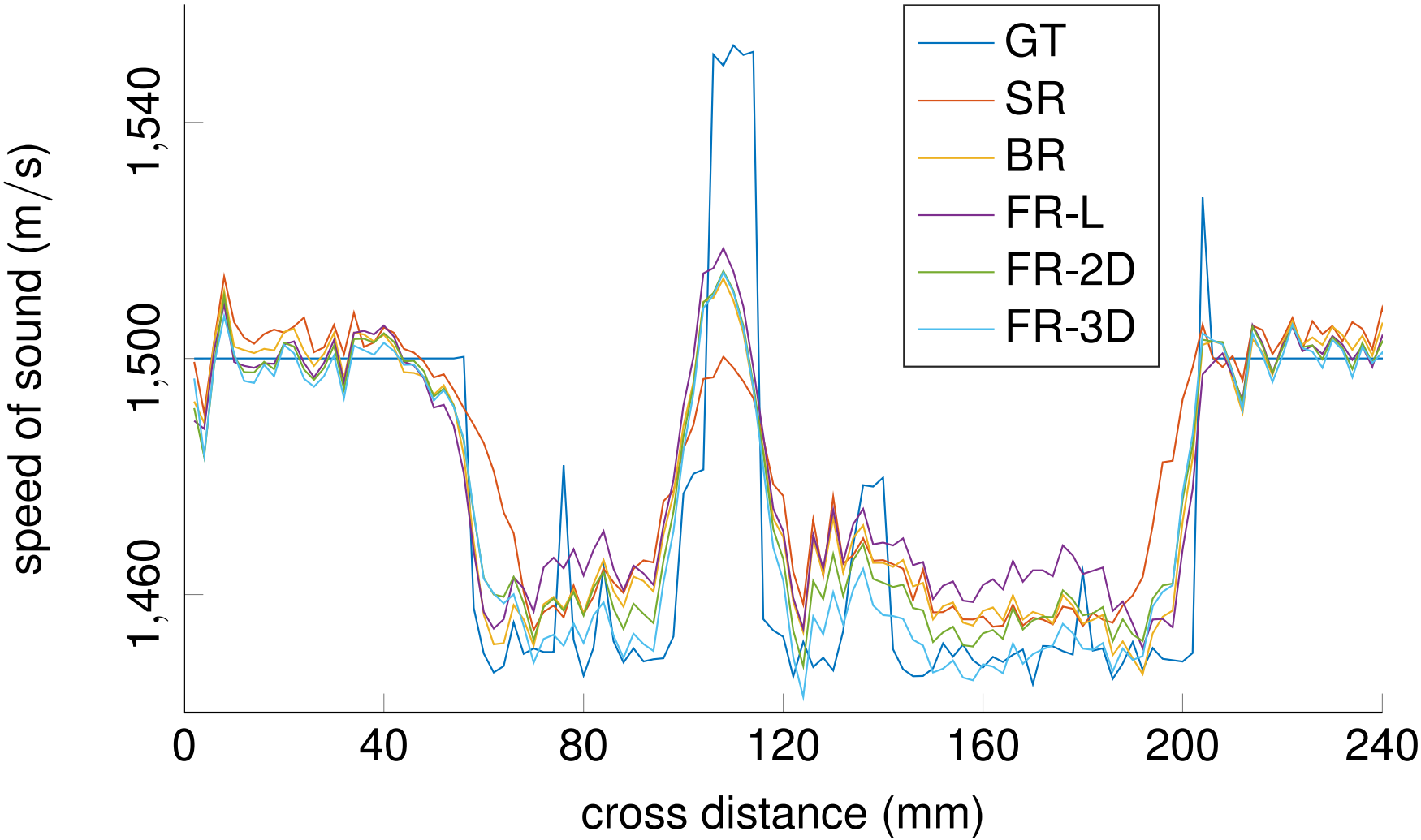

Figure 12: cross section of SART reconstruction ideal case

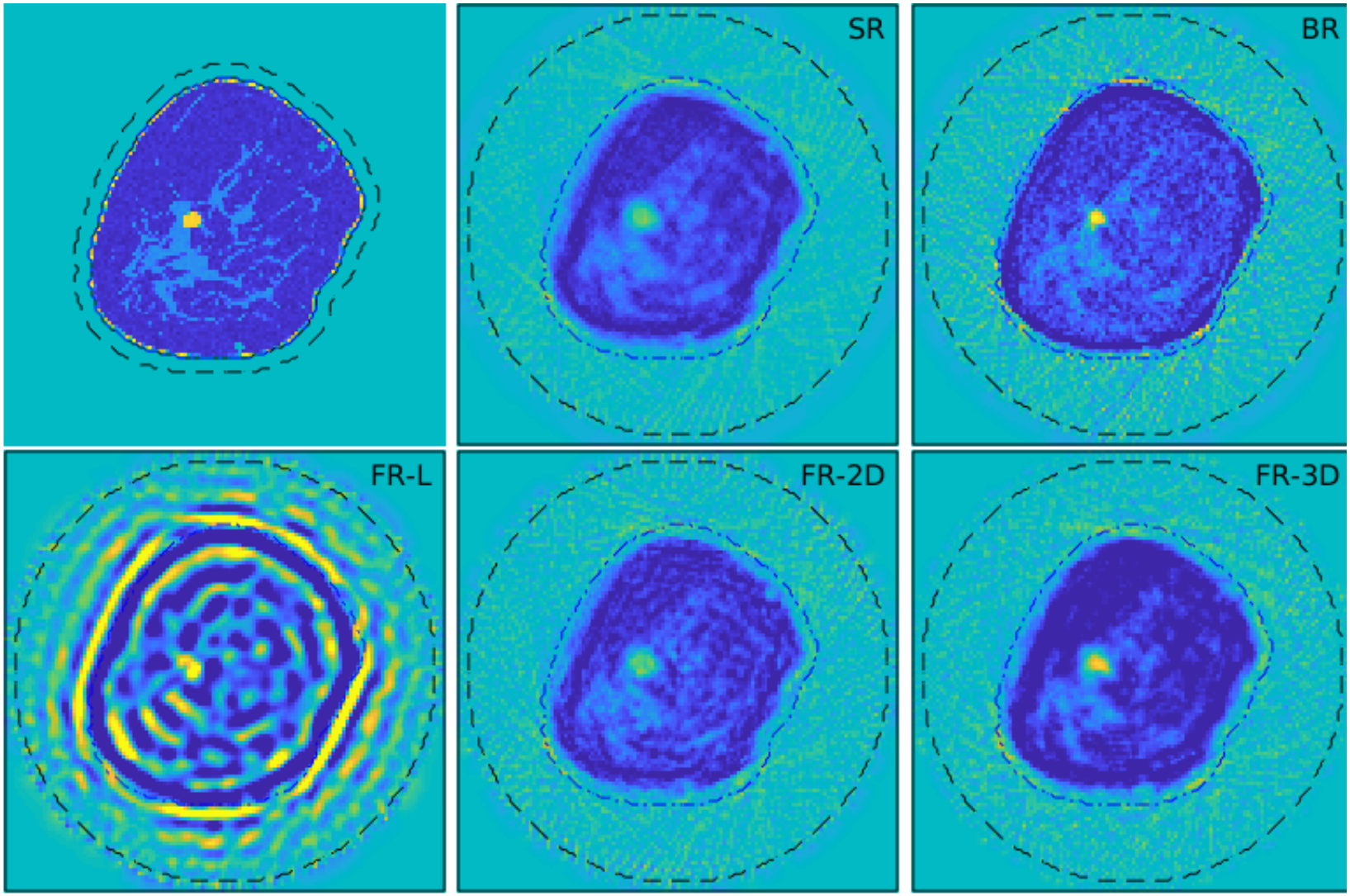

Figure 13: TVAL reconstruction, weak regularization on gradient ($\beta = 10^{-2}, \mu = 10^{3}$). 128 emitters, full opening angle.

Results

TVAL Regularisation

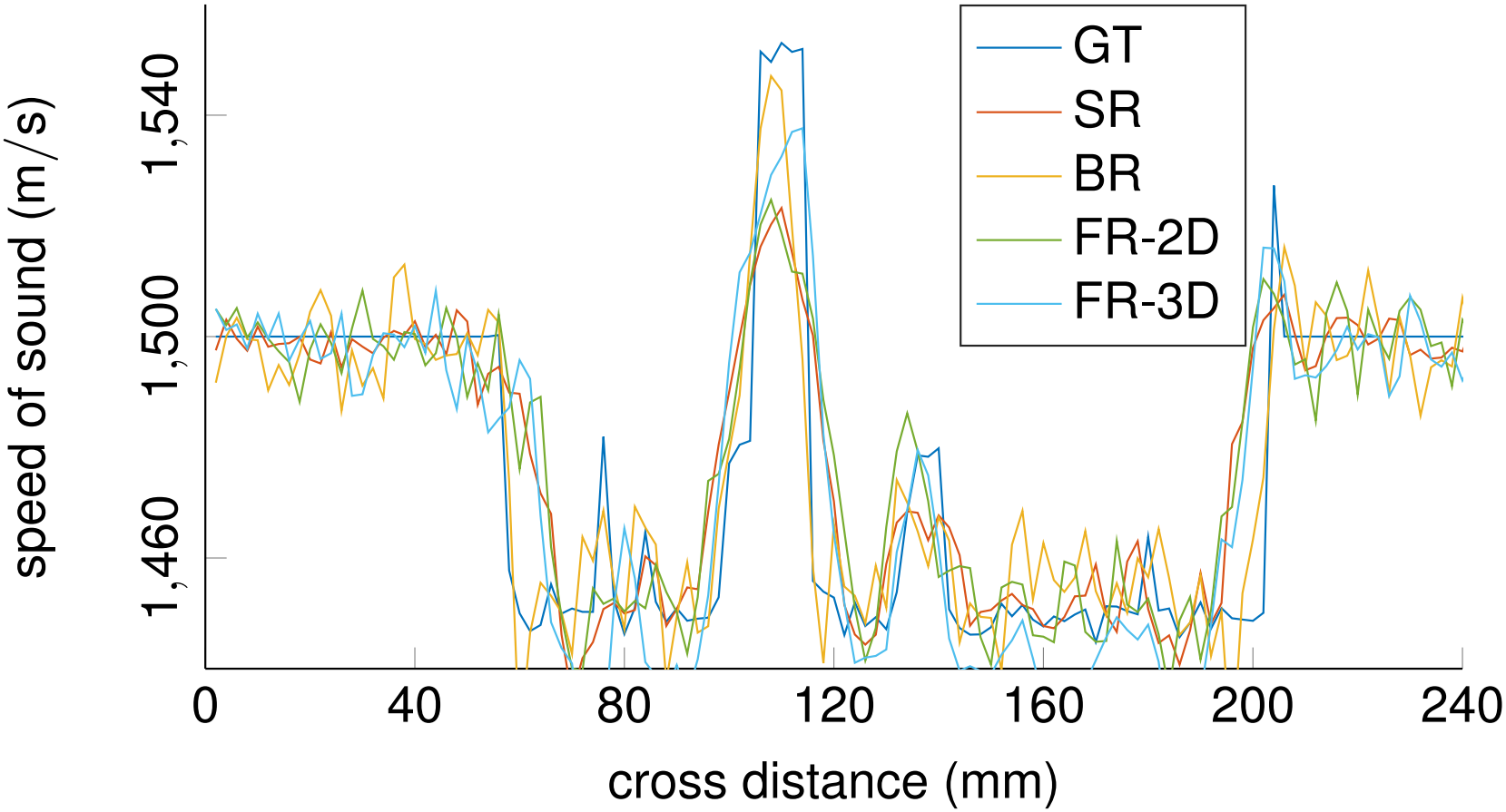

Figure 14: cross section of the TVAL reconstruction

3D reconstruction

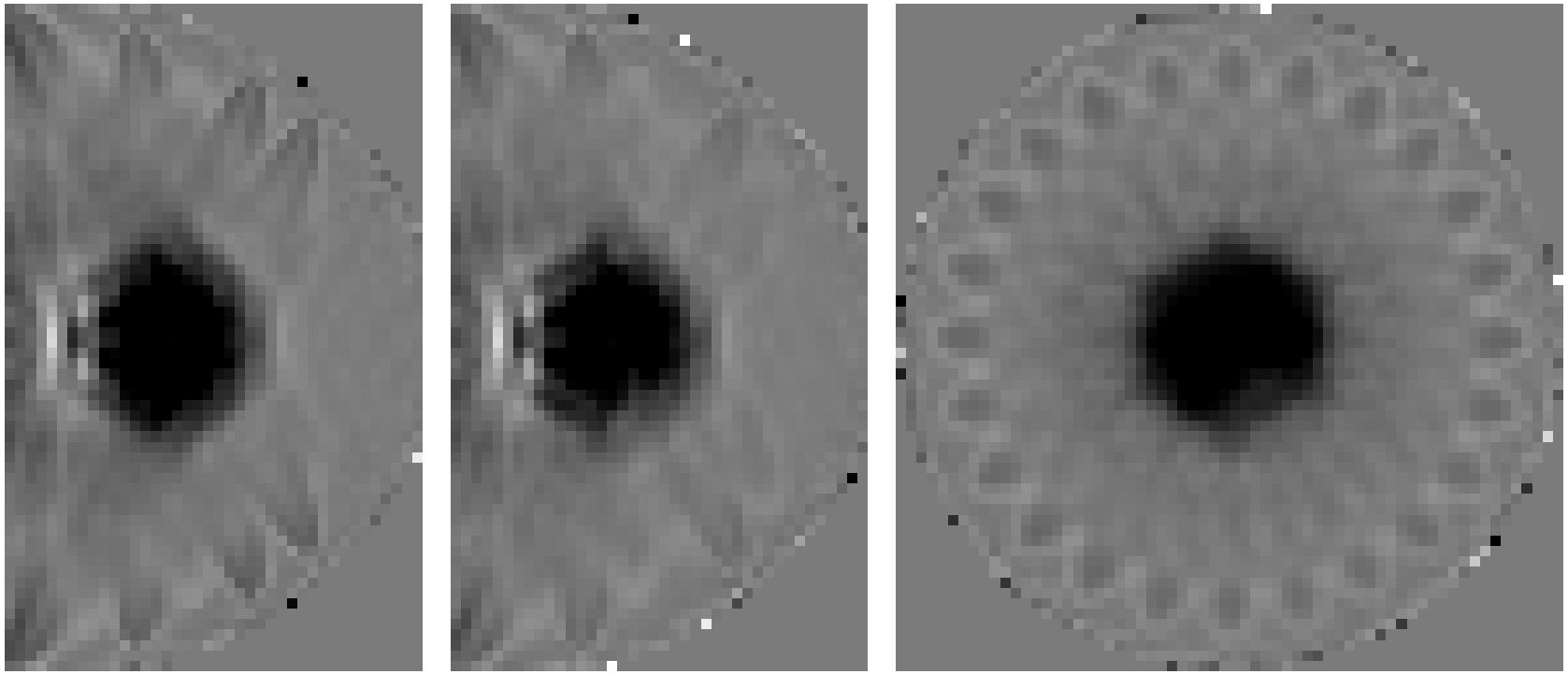

3D phantom (64x64x50) reconstruction. 1 emitter for 4 receiver

Fat Ray Linear, SART, No TV, no ROI

3D reconstruction

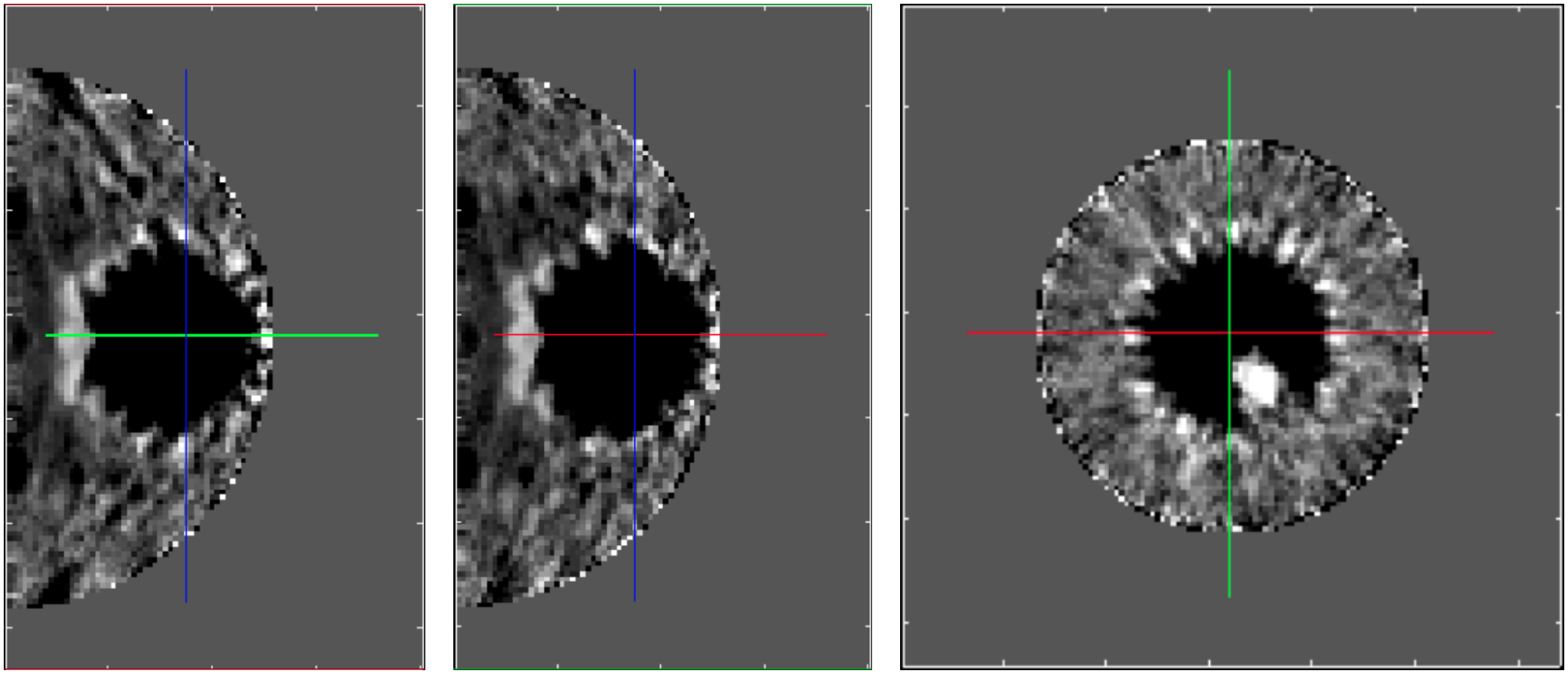

3D phantom (64x64x50) reconstruction. 1 emitter for 4 receiver

Fat Ray, SART, Strong TV, ROI

Conclusion & Future work

Achievements

- Fat Ray implementation
- ROI-based computation
- 3D simulation and Regularisation
- SART more robust than TVAL

Future work ?

- C-MEX / GPU Implementation
- Experimental Data

Thank you for listening

any questions ?

Fat Ray

Kernel expression

$$K_t^{3D}(\boldsymbol{y}) = \frac{s_0}{2\pi} \frac{\|\boldsymbol{x}_r - \boldsymbol{x}_e\|}{\|\boldsymbol{x}_r - \boldsymbol{y}\|\|\boldsymbol{y} - \boldsymbol{x}_e\|} \int_{\omega-\Delta\omega}^{\omega+\Delta\omega} A(\omega)\omega \sin(\omega s_0 \delta l(\boldsymbol{y}))\mathrm{d}\omega$$

$$K_t^{2D}(\boldsymbol{y}) = \sqrt{\frac{s_0}{2\pi}} \sqrt{\frac{\|\boldsymbol{x}_r - \boldsymbol{x}_e\|}{\|\boldsymbol{x}_r - \boldsymbol{y}\|\|\boldsymbol{y} - \boldsymbol{x}_e\|}} \int_{\omega-\Delta\omega}^{\omega+\Delta\omega} A(\omega)\sqrt{\omega} \sin\left(\omega s_0 \delta l(\boldsymbol{y}) + \frac{\pi}{4}\right) \mathrm{d}\omega$$

- Heavy computation
- Limits to Fresnel Zone
- No Hypothesis on slowness distribution
- Works also for attenuation

Solver design

SART vs TVAL3

SART

$$\boldsymbol{x}^{(k+1)} = \boldsymbol{x}^{(k)} + \lambda \boldsymbol{C}\boldsymbol{M}^T \boldsymbol{R}(\boldsymbol{y} - \boldsymbol{M}\boldsymbol{x}^{(k)})$$

With $\boldsymbol{C}$ and $\boldsymbol{R}$ diagonal matrices use for the ponderation:

$$c_{jj} = \left(\sum_{i=1}^{M} |M_{i,j}| \right)^{-1} \qquad r_{jj} = \left(\sum_{j=1}^{N} |M_{i,j}| \right)^{-1}$$

Solver design

SART vs TVAL3

TVAL3

Solve with total variation Regularisation:

$$\min \|\boldsymbol{D_x x}\|_1 + \|\boldsymbol{D_y x}\|_1 + \|\boldsymbol{D_z x}\|_1 \text{ with } \boldsymbol{y} = \boldsymbol{Mx}$$

$$\mathscr{L}(\beta, \mu, \boldsymbol{\lambda}, \boldsymbol{\nu}) = \underbrace{\sum_i \left(\|\boldsymbol{w}_i\| - \nu_i^T(\boldsymbol{D_i x} - \boldsymbol{w}_i) + \frac{\beta}{2}\|D_i \boldsymbol{x} - \boldsymbol{w}_i\|_2^2 \right)}_{\text{w-problem}} \tag{1}$$

$$\underbrace{- \boldsymbol{\lambda}^T(\boldsymbol{Mx} - \boldsymbol{b}) + \frac{\mu}{2}\|\boldsymbol{Mx} - \boldsymbol{b}\|_2^2}_{\text{x-problem}}$$

References and further readings

- [1] HOPP, T., ZUCH, F., COMBY, P. A., et al.*Fat ray ultrasound transmission tomography: preliminary experimental results with simulated data.*
- [2] GEMMEKE H., HOPP T., ZAPF M., et al.*3D ultrasound computer tomography: Hardware setup, reconstruction methods and first clinical results.*
- [3] `https://perso.crans.org/comby/ipe/report.pdf`